

**RECONSTRUCTING THIN SHAPES FROM
BOUNDARY ELECTRICAL MEASUREMENTS WITH LEVEL SETS**

By

D. Álvarez

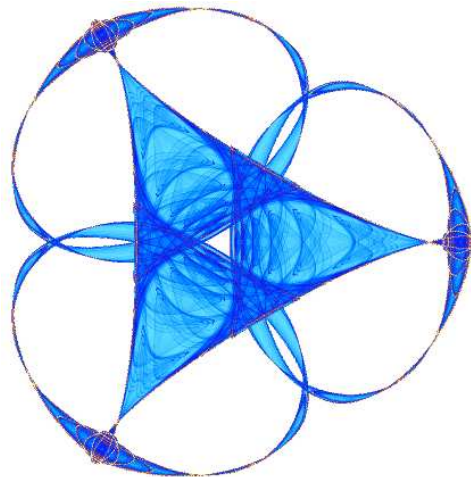
O. Dorn

and

M. Moscoso

IMA Preprint Series # 2127

(July 2006)



INSTITUTE FOR MATHEMATICS AND ITS APPLICATIONS

UNIVERSITY OF MINNESOTA
400 Lind Hall
207 Church Street S.E.
Minneapolis, Minnesota 55455-0436

Phone: 612/624-6066 Fax: 612/626-7370

URL: <http://www.ima.umn.edu>

RECONSTRUCTING THIN SHAPES FROM BOUNDARY ELECTRICAL MEASUREMENTS WITH LEVEL SETS

D. ÁLVAREZ, O. DORN, AND M. MOSCOSO

Abstract. We present a new technique for reconstructing thin shapes of fixed thickness from boundary electrical measurements. The main application which we have in mind is crack detection, but the approach is not limited to that. We introduce an extension of the level set technique for modelling thin shapes. Two level set functions are employed in order to achieve this: the first one models the location and form of the thin shape, and the second one models the length and connectivity of it. A gradient based method is derived in order to define evolution laws for these two level set functions which minimize the least squares data misfit. This evolution of the two level set functions corresponds to an evolution of the thin shape or crack during the reconstruction. We present numerical experiments which demonstrate that our technique is able to recover disconnected thin shapes or cracks from noisy simulated boundary data.

Key Words. level sets, cracks, thin shapes, electrical impedance tomography

1. Introduction

There exist many practical problems for which it is necessary to retrieve the electrical properties of a medium from measured data at its boundary. Among others, we mention here clinical applications such as electrical impedance tomography (EIT) [19, 10], geophysical applications such as determining the location of mineral deposits in the earth or monitoring the propagation of contaminants [3, 12, 13, 23, 29, 30], and industrial applications such as non-destructive testing [4, 15, 31, 35]. It is well known that all these applications lead to inverse problems that are usually severely ill-posed. Therefore, it is desirable to make use of available a priori information in order to regularize and stabilize the reconstruction of the properties of the medium.

In this paper we focus on the identification of thin shapes, where we are aiming mainly at the application of crack detection, even though the discussion will not be limited to that. These thin shapes are assumed here to be thin regions of fixed thickness and known electrical properties. However, their location, form and connectivity structure is assumed to be unknown, which means that the crack could consist of two (or more) different parts which are disconnected. The electrical properties inside the crack are assumed to be sufficiently different from the background material, with a contrast of a factor 2 to 5, for example. We do not consider cracks which are impenetrable (i.e. perfectly insulating cracks).

Our main purpose in this paper is to investigate a novel shape-based reconstruction algorithm that uses a level set technique. Level sets, originally introduced in [27], have been widely used for solving inverse problems since the seminal work in [33]. We refer to the early works [33, 23, 17, 13, 8, 20, 30] and to the recent review

[14] for an overview on level set techniques applied to inverse problems. However, so far, level set methods have not yet been applied successfully to the reconstruction of thin cracks, mainly due to the fact that traditional level set techniques are tailored to describing volumetric objects rather than thin regions (see, for example, the related work [9, 11, 16, 20, 35, 36, 37]). It is our goal to present here one possible extension of the level set technique which still assumes the objects (cracks) to have a volumetric interior (which means their thickness is still finite instead of converging to zero) but which are sufficiently thin. Due to the small thickness the object can not easily be described by traditional level set techniques. With the above mentioned assumptions, we can model the evolution of the cracks in both directions, in the normal and in the tangential direction of the crack, by some appropriate adaptations of classical tools to this new situation. The normal component evolution will correspond to the movement of the crack over the domain, whereas the tangential evolution will change length and connectivity of the crack.

Friedman and Vogelius studied in [18] the uniqueness of the crack detection problem from electrical boundary measurements and they show that perfectly insulating cracks can be uniquely identified from appropriately collected boundary measurements. Previously, Kohn and Vogelius had considered the retrieval of a finite number of cavities [21], and Nachman studied the case of spatially varying smooth electric properties [24, 25]. Later, Santosa and Vogelius proposed a reconstruction algorithm specifically designed for locating a single crack [32, 22]. The algorithm was generalized to the location of multiple cracks in [7]. Alessandrini and coauthors focused on different uniqueness and stability issues in [1, 2]. More recent work on the recovery of insulating cracks can be found in [5]. We refer to the review [6] for more details and references about theoretical and computational aspects about the problem of crack detection.

The paper is organized as follows. In section 2 we will discuss the forward model which we will use for our study, which is the application of electrical fields for the detection of thin shapes. In section 3 we explain our novel approach for representing thin shapes by a pair of two level set functions. Section 4 briefly states some classical material on how to calculate Fréchet derivatives in this situation by an adjoint technique. In section 5 we outline how to evolve the first of the two level set functions, being responsible for location and form of the crack, by using a gradient-based scheme which reduces the data least squares misfit cost functional. Section 6 completes the gradient calculation by considering evolution of the second level set function, being responsible for connectivity and length of the crack. In Section 7 we summarize our numerical algorithm for the reconstruction of the shapes. In Section 8 we present several numerical experiments which demonstrate the performance of our new algorithm, and section 9 contains our conclusions and some hints to future work.

2. The forward problem

We assume in this paper that the electric field \mathbf{E}_j inside the medium for an applied boundary potential γ_j can be described as $\mathbf{E}_j(\mathbf{x}) = -\nabla u_j(\mathbf{x})$ where u_j is an electric potential function with

$$(1) \quad \nabla \cdot b(\mathbf{x})\nabla u_j = 0 \quad \text{in } \Omega,$$

and satisfying the boundary condition

$$(2) \quad u_j = \gamma_j \quad \text{on } \partial\Omega.$$

The quantity of interest for the inverse problem is the conductivity $b(\mathbf{x})$. For our theoretical considerations below we will, for simplicity of notation, assume that $\Omega = [0, 1] \times [0, 1]$ is the unit square. This assumption is not necessary for the validity of our method.

In this paper we are in particular interested in the situation where the conductivity profile $b(\mathbf{x})$ contains sharp (but finite) jump discontinuities at interfaces between a crack-like shape (having conductivity value b_i) and the background material (having conductivity value b_e). In this situation, the correct interface jump conditions are

$$(3) \quad \left[\left[b \frac{\partial u_j}{\partial n} \right] \right] = 0 \quad , \quad \left[[u_j] \right] = 0$$

at the interior interfaces. In (3) we have used the notation $\left[[w] \right] = w_e - w_i$, where w_e and w_i mean the exterior and interior limits of the quantity w at the interfaces, respectively.

Given a source (i.e., applied boundary condition) γ_j , the corresponding physical measurements are given by

$$(4) \quad g_{jl} = \frac{\partial u_j}{\partial n}(d_l)$$

taken at positions $d_l \in \partial\Omega$ for $l = 1, \dots, \underline{l}$ where u_j solves (1), (2) for the given source. Denoting $g_j = \{g_{jl}\}_{l=1, \dots, \underline{l}}$, we write this as

$$(5) \quad \mathcal{A}_j(b) = g_j = \mathcal{M}_j u_j$$

where we have introduced the linear measurement operator \mathcal{M}_j . We let the actually measured (or 'true') data \tilde{g}_j be such that

$$(6) \quad \tilde{g}_j = \mathcal{M}_j \tilde{u}_j,$$

where \tilde{u}_j denotes the unknown physical states for the correct parameter distribution \tilde{b}_j . The 'residual operators' \mathcal{R}_j are now defined by

$$(7) \quad \mathcal{R}_j(b) = \mathcal{A}_j(b) - \tilde{g}_j.$$

3. Representing thin shapes by two level set functions

We assume that we have given a continuously differentiable level set function $\varphi(\mathbf{x}) = \varphi(x, y)$ [28, 34]. We define a thin region represented by this level set function in the following way. Let be

$$(8) \quad \Omega_1 = \{(x, y) \in \mathbf{R}^2 : \varphi(x, y) \leq 0\},$$

$$(9) \quad \Gamma_1 = \{(x, y) \in \mathbf{R}^2 : \varphi(x, y) = 0\}.$$

Here, Γ_1 is the zero level set. The outward normal \mathbf{n} to Γ_1 is given by

$$(10) \quad \mathbf{n}(\mathbf{x}) = \frac{\nabla\varphi(\mathbf{x})}{|\nabla\varphi(\mathbf{x})|} \quad \text{on } \Gamma_1.$$

We define now the thin region D of width $\epsilon > 0$ to be

$$(11) \quad D = \Omega_1 \cap \{\mathbf{y} \in \mathbf{R}^2 : \text{there exist } \mathbf{x} \in \Gamma_1 \text{ such that } \mathbf{y} = \mathbf{x} - \alpha\mathbf{n}(\mathbf{x}), \text{ for some } 0 \leq \alpha \leq \epsilon\}.$$

In addition we define $\Gamma_2 = \partial D \setminus \Gamma_1$ (see Figure 1). With these definitions, a given level set function φ uniquely specifies a thin region $D[\varphi, \epsilon]$ of thickness ϵ . Since the thickness ϵ will be fixed throughout this paper, we will omit it in the notation and simply write $D[\varphi]$.



FIGURE 2. A broken thin shape defined by two level set functions.

4. Pixel-based gradient calculation

We define the least squares cost functional

$$(15) \quad \mathcal{J}_j(b) = \frac{1}{2} \|\mathcal{R}_j(b)\|_Z^2 = \frac{1}{2} \langle \mathcal{R}_j(b), \mathcal{R}_j(b) \rangle_Z$$

where $\langle \cdot, \cdot \rangle_Z$ denotes the canonical inner product in data space Z . We assume that $\mathcal{R}_j(b)$ admits the expansion

$$(16) \quad \mathcal{R}_j(b + \delta b) = \mathcal{R}_j(b) + \mathcal{R}'_j(b)\delta b + O(\|\delta b\|_P^2),$$

letting $\|\cdot\|_P$ be the canonical norm in parameter space P , for a sufficiently small perturbation (variation) $\delta b \in P$. The linear operator $\mathcal{R}'_j(b)$ (if it exists) is often called the *Fréchet derivative* of \mathcal{R}_j . Plugging (16) into (15) yields the relationship

$$(17) \quad \mathcal{J}_j(b + \delta b) = \mathcal{J}_j(b) + \langle \mathcal{R}'_j(b)^* \mathcal{R}_j(b), \delta b \rangle_P + O(\|\delta b\|_P^2).$$

The operator $\mathcal{R}'_j(b)^*$ is the formal adjoint operator of $\mathcal{R}'_j(b)$ with respect to spaces Z and P :

$$(18) \quad \langle \mathcal{R}'_j(b)^* g, \hat{b} \rangle_P = \langle g, \mathcal{R}'_j(b) \hat{b} \rangle_Z \quad \text{for all } \hat{b} \in P, g \in Z.$$

We call

$$(19) \quad \mathbf{grad}_{\mathcal{J}_j}(b) = \mathcal{R}'_j(b)^* \mathcal{R}_j(b)$$

the *gradient direction* of \mathcal{J}_j in b .

The following adjoint formulation for calculating pixel-based gradient directions is well-known and easy to derive, see [3, 26]. We give here the main result.

Let ζ be an element in data space Z . Then, $\mathcal{R}'_j(b)^* \zeta$ is given by

$$(20) \quad \mathcal{R}'_j(b)^* \zeta = \nabla u_j \cdot \nabla z_j,$$

where u_j solves (1)-(2) and z_j solves the following adjoint equation

$$(21) \quad \nabla \cdot b \nabla z_j = 0 \quad \text{in } \Omega,$$

$$(22) \quad b z_j = \zeta \quad \text{on } \partial\Omega.$$

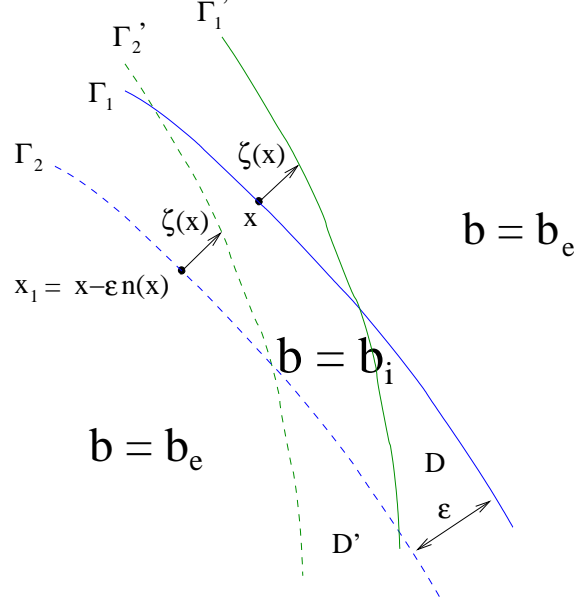


FIGURE 3. Moving a thin shape by level sets.

Defining the total cost

$$(23) \quad \mathcal{J}(b) = \sum_{j=1}^j \mathcal{J}_j(b)$$

we get the combined gradient direction

$$(24) \quad \mathbf{grad}_{\mathcal{J}}(b) = \sum_{j=1}^j \mathbf{grad}_{\mathcal{J}_j}(b) = \sum_{j=1}^j \mathcal{R}'_j(b) * \mathcal{R}_j(b).$$

5. Deformation of thin shapes with level sets

In this section we want to define a shape evolution which gradually deforms an initial shape into a descent direction with respect to the cost (24) until the cost is minimized. The final shape will provide us with the solution of our inverse problem.

In our situation we want to move the thin shape in a very restricted way such that it always remains a thin shape as defined in the previous sections.

When moving every point $\mathbf{x} \in \Gamma_1$ a small (infinitesimal) displacement $\zeta(\mathbf{x})$, the boundary Γ_1 will be deformed (see Figure 3). In order to move the complete thin region, we will now extend this displacement field from Γ_1 into D in the following way: By construction, every point $\mathbf{y} \in D$ can be written in the form $\mathbf{y} = \mathbf{x} - \alpha \mathbf{n}(\mathbf{x})$ for at least one $\mathbf{x} \in \Gamma_1$ and some $0 \leq \alpha \leq \epsilon$. For simplicity we assume here that both, \mathbf{x} and α are uniquely defined by the value \mathbf{y} . Then, we assume that every point $\mathbf{y} \in D$ moves the same distance and direction (i.e. by the same displacement ζ) as its reference point $\mathbf{x} \in \Gamma_1$. In particular, this holds true for all points $\mathbf{x}_1 \in \Gamma_2$. (In fact, we can approximate locally each boundary element on Γ_1 by a straight line, which can be extended to an infinitesimal rectangle toward Γ_2 by the process described in (11). Then, all points inside this infinitesimal rectangle move the same distance and direction.)

In order to find the change in the cost $\mathcal{J}(b)$ due to the above described deformation of the thin shape, we will follow the line of reasoning given in [33] and will adapt it to this new situation. This will be done in our analysis by making use of the just mentioned relation between points moving on Γ_1 and those moving on Γ_2 .

To start with, we observe (see [14, 33] for details) that the movement of Γ_1 gives rise to the parameter change

$$(25) \quad \delta b_1 = (b_i - b_e) \mathbf{n}(\mathbf{x}) \cdot \zeta(\mathbf{x}) \delta_{\Gamma_1}(\mathbf{x}) \chi_B(\mathbf{x})$$

with δ_{Γ_1} being the Dirac delta distribution concentrated on Γ_1 and $\chi_B(\mathbf{x}) = h(-\psi(x))$ being the characteristic function of the band structure B (the symbol h denoting the Heaviside function). In our model, a deformation of Γ_1 is automatically combined with a corresponding deformation of Γ_2 as described before. This will give rise to an additional contribution in the change of the parameter distribution, namely

$$(26) \quad \delta b_2 = (b_i - b_e) \mathbf{n}(\mathbf{x}) \cdot \zeta(\mathbf{x}) \delta_{\Gamma_2}(\mathbf{x}) \chi_B(\mathbf{x}).$$

Summing up the two contributions, we get the total change of parameters

$$(27) \quad \delta b = (b_i - b_e) \mathbf{n}(\mathbf{x}) \cdot \zeta(\mathbf{x}) \left[\delta_{\Gamma_1}(\mathbf{x}) + \delta_{\Gamma_2}(\mathbf{x}) \right] \chi_B(\mathbf{x}).$$

A descent direction with respect to our cost functional can be calculated by plugging (27) into (17). We get

$$(28) \quad \mathcal{J}_j(b + \delta b) = \mathcal{J}_j(b) + \left\langle \mathcal{R}'_j(b) * \mathcal{R}_j(b), (b_i - b_e) \mathbf{n}(\mathbf{x}) \cdot \zeta(\mathbf{x}) \left[\delta_{\Gamma_1}(\mathbf{x}) + \delta_{\Gamma_2}(\mathbf{x}) \right] \chi_B(\mathbf{x}) \right\rangle_P + O(\|\delta b\|_P^2).$$

So far we have not yet used the fact that we only want to find a descent direction for points \mathbf{x} on Γ_1 . The corresponding points $\mathbf{x}_1 = \mathbf{x} - \epsilon \mathbf{n}(\mathbf{x}) \in \Gamma_2$ will move automatically as described above, such that their influence on the cost functional will be incorporated in the contributions of the points of Γ_1 . In order to establish this link, we write now the linear term of (28) explicitly using the standard L_2 inner product in P and replacing the terms which correspond to Γ_2 by their counterparts on Γ_1 using the above described rules. This yields

$$(29) \quad \begin{aligned} \delta \mathcal{J}_j(b) &= \int_{\mathbb{R}^2} \mathcal{R}'_j(b) * \mathcal{R}_j(b) (b_i - b_e) \mathbf{n}(\mathbf{x}) \cdot \zeta(\mathbf{x}) \left[\delta_{\Gamma_1}(\mathbf{x}) + \delta_{\Gamma_2}(\mathbf{x}) \right] \chi_B(\mathbf{x}) dx \\ &\approx \int_{\Gamma_1} (b_i - b_e) \mathbf{n}(\mathbf{x}) \cdot \zeta(\mathbf{x}) \left[\mathcal{R}'_j(b) * \mathcal{R}_j(b)(\mathbf{x}) - \mathcal{R}'_j(b) * \mathcal{R}_j(b)(\mathbf{x} - \epsilon \mathbf{n}(\mathbf{x})) \right] \chi_B(\mathbf{x}) ds \end{aligned}$$

where we have used that $\zeta(\mathbf{x}) = \zeta(\mathbf{x} - \epsilon \mathbf{n}(\mathbf{x}))$ and $\mathbf{n}(\mathbf{x}) = -\mathbf{n}(\mathbf{x} - \epsilon \mathbf{n}(\mathbf{x}))$ by construction. Moreover, we have assumed that $\chi_B(\mathbf{x}_1) \approx \chi_B(\mathbf{x})$.

Let us specify now the displacement $\zeta(\mathbf{x})$ to be given as

$$(30) \quad \zeta(\mathbf{x}) = F(\mathbf{x}) \mathbf{n}(\mathbf{x}) \tau$$

for some scalar velocity function $F(\mathbf{x})$ defined on Γ_1 and some time step τ . This amounts to the movement of points $\mathbf{x} \in \Gamma_1$ by the vector velocity field $\mathbf{V}(\mathbf{x}) = F(\mathbf{x}) \mathbf{n}(\mathbf{x})$. Plugging this into (29) we get the descent velocity

$$(31) \quad F_d(\mathbf{x}) = -(b_i - b_e) \left[\mathcal{R}'_j(b) * \mathcal{R}_j(b)(\mathbf{x}) - \mathcal{R}'_j(b) * \mathcal{R}_j(b)(\mathbf{x} - \epsilon \mathbf{n}(\mathbf{x})) \right] \chi_B(\mathbf{x}) \quad \text{on } \Gamma_1.$$

Letting $\tau \rightarrow 0$, and choosing a suitable extension velocity outside Γ_1 , we arrive at an evolution equation for the level set function φ which describes motion of Γ_1 in a

descent direction to the least squares cost functional $\mathcal{J}_j(b)$. It is of Hamilton-Jacobi type (see [14])

$$(32) \quad \frac{\partial \varphi}{\partial t} + F_d |\nabla \varphi| = 0$$

where F_d is given by (31). An analogous result holds for the total cost $\mathcal{J}(b)$, summing up contributions of individual sources γ_j . A finite-difference time-discretization of (32) gives us the iteration rule for updating the level set function in each time step. It is

$$(33) \quad \varphi^{(n+1)} = \varphi^{(n)} + \tau_\varphi F_d^{(n)} |\nabla \varphi^{(n)}|, \quad \varphi^{(0)} = \varphi_0,$$

with step-size $\tau_\varphi > 0$ which can be chosen fixed or, alternatively, determined by some line-search criterion.

6. Estimating length and connectivity of the thin shape

So far we only have calculated descent directions of the first level set function φ with respect to the least squares cost (23). However, the thin structures which we want to find will have a finite length and they might consist of more than one components. We will also have to determine the second level set function ψ from the given data in order to specify this additional property. In the following we describe how we achieve this goal.

Denote by Γ_B the set $\{\mathbf{x} = (x, y) \in \mathbb{R}^2, \psi(x) = 0\}$. Obviously, Γ_B is just the boundary of B , $\Gamma_B = \partial B$, and its outward normal is given as $\mathbf{n}_B = \pm \mathbf{e}_x$, where \mathbf{e}_x is the cartesian unit vector in direction x . The sign will depend on the specific point $\mathbf{x} \in \partial B$ which we consider. Following the same arguments as in the previous section, we see immediately that a displacement $\mathbf{x} \rightarrow \mathbf{x} + \xi(x) \mathbf{n}_B(\mathbf{x})$ in the outward normal direction will give rise to a parameter change

$$(34) \quad \delta b_B(x, y) = (b_i - b_e) \xi(x) \delta_{\Gamma_B}(x, y) \chi_D(x, y),$$

where $\chi_D(x, y)$ denotes the characteristic function of the thin region D . Plugging this into (17), we calculate the linearized response in the cost as

$$(35) \quad \delta \mathcal{J}_j = \left\langle \mathcal{R}'_j(b) * \mathcal{R}_j(b), (b_i - b_e) \xi(x) \delta_{\Gamma_B}(x, y) \chi_D(x, y) \right\rangle_P.$$

Notice that $\xi(x)$ does only depend on the first variable of $\mathbf{x} = (x, y)$. We write $\xi(x) = F_B(x) \tau_\psi$ for some velocity field $F_B(x)$ and a time-step $\tau_\psi > 0$. Using the canonical L_2 inner product in (35) we get

$$(36) \quad \delta \mathcal{J}_j = \tau_\psi \int F_B(x) \left(\int \mathcal{R}'_j(b) * \mathcal{R}_j(b) (b_i - b_e) \delta_{\Gamma_B}(x, y) \chi_D(x, y) dy \right) dx,$$

such that we find the descent direction

$$(37) \quad F_{B,d}(x) = - \int \mathcal{R}'_j(b) * \mathcal{R}_j(b) (b_i - b_e) \delta_{\Gamma_B}(x, y) \chi_D(x, y) dy \quad \text{at } \Gamma_B.$$

In fact, in our numerical experiments we will choose the extension velocity such that (37) is applied not only on Γ_B but for all $x \in [0, 1]$. This allows for breaking a shape into two parts at points far away from the current boundary by raising a negative valued level set function in some region until the values become positive. See, for example, the detailed discussion in [14]. The iteration for the second level set function ψ reads now

$$(38) \quad \psi^{(n+1)} = \psi^{(n)} + \tau_\psi F_{B,d}^{(n)} |\nabla \psi^{(n)}|, \quad \psi^{(0)} = \psi_0.$$

7. Numerical algorithm for the reconstruction

In the following, we briefly summarize the algorithm which we have developed for finding and characterizing thin shapes (cracks) from boundary data. It will be tested in our numerical experiments described in section 8 on the experimental setup as outlined in section 2.

We denote again the source (or applied boundary condition) by γ_j and the corresponding physical measurements by g_{jl} (4), which are taken at positions $d_l \in \partial\Omega$ for $l = 1, \dots, L$. The fields u_j satisfy (1)-(2) for the given source. We will use a straightforward finite differences scheme of (1)-(2) for our forward modelling.

The basic numerical algorithm can now be summarized as follows. Let us assume that the n th approximation to the level functions $\varphi^{(n)}(\mathbf{x})$ and $\psi^{(n)}(x)$ has been obtained in previous steps of this algorithm. The corresponding parameter distribution is $b^{(n)}(\mathbf{x})$. Then, we continue by:

- (1) For each source γ_j , we calculate the residual $\zeta_j = g_{jl}^{(n)} - \tilde{g}_{jl}$, where $g_{jl}^{(n)}$ is the data of forward problem (1)-(2) using as electrical conductivity $b^{(n)}$.
- (2) We solve the adjoint problem (21)-(22) and calculate

$$\mathcal{R}'_j(b) * \mathcal{R}_j(b) = \nabla u_j \cdot \nabla z_j.$$

- (3) We use (31) for computing $F_d(\mathbf{x})$, and (37) for computing $F_{B,d}(x)$.
- (4) We apply some additional regularization (smoothing the obtained contributions $F_d(\mathbf{x})$ and $F_{B,d}(x)$) as explained in [14].
- (5) We correct the level set functions $\varphi^{(n)}$ and $\psi^{(n)}$ according to (33) and (38), respectively. The step-sizes are chosen empirically prior to starting the algorithm.
- (6) We determine the new parameter function $b^{(n+1)}(\mathbf{x})$ according to (14).

We stop this process according to some stopping criterion, for example at a maximal number of iterations or at a point where the cost becomes practically stationary, i.e., oscillates around some value without decreasing further for some time.

The algorithm is initialized by specifying some initial functions $\varphi^{(0)}(\mathbf{x})$ and $\psi^{(0)}(x)$.

8. Numerical experiments

In the numerical experiments shown here, the domain of investigation consists of a square of size $1 \times 1\text{m}^2$ in which a thin object will be embedded at various positions for testing the algorithm. The thickness of this thin object is $(3/50)\text{m}$. The conductivity values are 0.75 Siemens/m (S/m) in the background and 0.25 S/m inside the thin object. 11 sources are equidistantly located at each side of the square, such that the total number of sources is 44. Each source applies a potential of 1 Volt. The receivers are located at the same positions as the sources, where we assume that all receivers collect data for a given active source position. We solve equations (1)-(2) with a classical second order finite differences scheme on a numerical grid of size 50×50 .

The data on the boundary are generated in the following way. We set u_j equal to one at the boundary node where the source with number j is located, and to zero elsewhere on $\partial\Omega$. For the data generation, we solve the direct problem (1), (2) on the true reference profile.

In our first numerical experiment, we consider a single thin object in the domain. No noise is added to the data in this example. The initial guess and the evolution of

the reconstruction after 20, 50, 70, 100, and 150 iterations are displayed in the first and second rows of Figure 4. The final reconstruction after 200 iterations is shown in the left image of the third row in the same figure. The reference medium is plotted in the center image of that row. We observe in the bottom right image, which shows the evolution of the cost, that the cost decreases during this evolution of the shape approximately until iteration 180, and then remains practically constant. This could be used as a stopping criterion of our algorithm, even though in the experiments presented here we apply a fixed maximal number of iterations in order to observe the general behavior of the algorithm. From this numerical experiment we conclude that our algorithm is able to estimate the position, form and length of a single thin object quite well.

In order to show that the algorithm is also able to reconstruct an object which is composed of several components as shown in the top left image of Figure 6, we have displayed the shape evolution corresponding to this situation in Figure 5. The figure shows the initial guess (top left image) as well as the reconstructions after 10, 30, 40, 50, 60, 70, 120 and 150 iterations. Comparing the final result with the reference medium in the top left image of Figure 6, we can see that the algorithm is in fact able to recover and distinguish the two different components of the thin shape, and that it predicts the general orientation and lengths of these individual components well.

We have also investigated the behavior of our algorithm when noise is added to the data. Here we used Gaussian noise which was added to the real data \tilde{g}_j , with the effect that $\tilde{g}_j \rightarrow \tilde{g}_j(1 + \sigma\Theta)$, where Θ is a normal distribution of mean zero and standard deviation 1. In Figure 6 we show the final reconstruction after 200 iterations for different values for σ . The reference medium is again displayed in the top left image of the figure, and the reconstruction after 200 iterations with no noise is displayed in the top right image. The reconstructions after 200 iterations with noisy data corresponding to $\sigma = 0.001$ (which amounts to 0.1 %) is shown in the bottom left image, and with $\sigma = 0.005$ (which amounts to 0.5 %) in the bottom right of the figure. Comparing the results, we conclude that, for the noise levels tested here, the reconstructions do not differ significantly. This indicates a reasonably good stability of our algorithm with respect to noise in the data.

In Figure 7 we show furthermore the evolution of the least squares cost for different noise levels. As it is expected, a higher noise level gives rise to a larger final residual value at which the evolution becomes stationary.

9. Conclusions and future work

We have presented a novel technique for finding and characterizing hidden thin shapes (or cracks) from electrical measurements at the boundary. A variant of a level set technique is developed in order to numerically modelling and propagating the thin shape. Two level set functions are employed for this purpose. The first one specifies the location and form of the thin shape, whereas the second one specifies its length and connectivity. A gradient technique has been developed for finding evolution laws for these two level set functions which simultaneously reduce the least squares data misfit cost functional. Numerical experiments have been presented which demonstrate that our new method is able to recover connected and disconnected thin shapes (cracks) from noisy simulated electrical boundary data. The conductivity values of background material and inside the cracks are assumed to be known, and differ in our numerical experiments by a factor 3. In particular, the cracks (thin shapes) have been assumed to be penetrable.

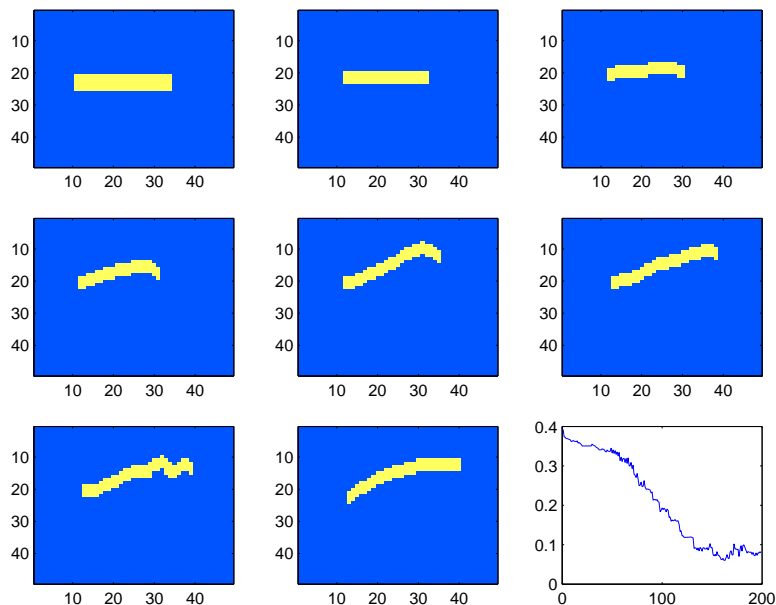


FIGURE 4. First numerical experiment: reconstruction of a single thin object. Upper row from left to right: initial guess, after 20, and 50 iterations. Central row from left to right: after 70, 100, and 150 iterations. Bottom row from left to right: final reconstruction after 200 iterations; reference medium; evolution of the least squares cost.

So far we have limited our investigation to situations of low contrast cracks. In our future research, we plan to investigate also high contrast situations using more sophisticated forward modelling tools. As additional interesting topics for future research we want to mention here the simultaneous reconstruction of the thin shape and the conductivity value inside this shape. Moreover, also the thickness of the thin shape can be included in the set of unknowns for the inverse problem, with the goal to simultaneously recover it from the given data.

Acknowledgments

This research was supported by the Spanish MCyT Grant No. BFM2002-04127-C02-01. Oliver Dorn is grateful for partial support by the IMA, Minneapolis.

References

- [1] Alessandrini G and DiBenedetto E 1997 Determining 2 dimensional cracks in 3 dimensional bodies: Uniqueness and stability, *Indiana Univ. Math. J* **46** 1–82
- [2] Alessandrini G and Rondi L 1998 Stable determination of a crack in a planar inhomogeneous conductor, *Siam J. Cont Opt* ,**34**(3) 913–921
- [3] Borcea L 2002 Electrical impedance tomography *Inverse Problems* **18** R99–R136.
- [4] Bowler J 2002 Thin-skin eddy-current inversion for the determination of crack shapes *Inverse Problems* **18**, 1891–1905.
- [5] Brühl M, Hanke M and Pidcock M 2001 Crack detection using electrostatic measurements *Math. Model. Numer. Anal.* **35** 595–605.
- [6] Bryan K and Vogelius M 2004 A review of selected works on cracks identification *Geom. Meth. in Inverse Problems and PDE Control IMA* **137** Springer-Verlag.

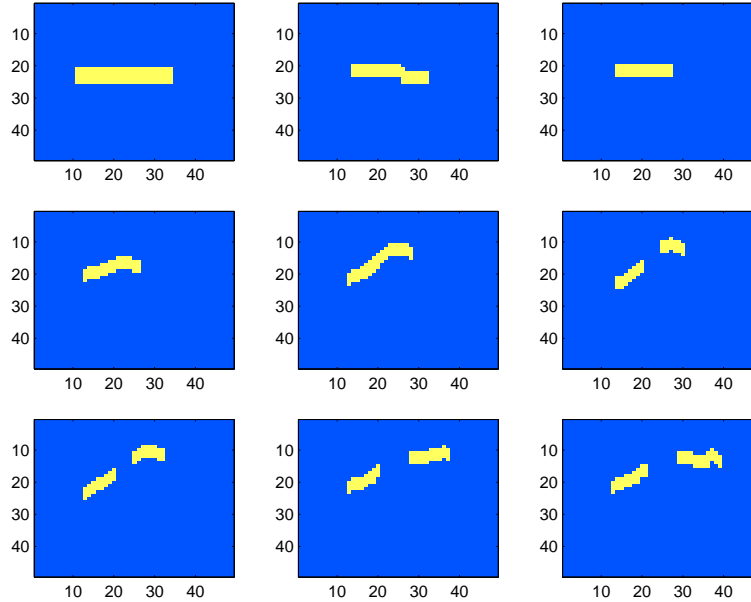


FIGURE 5. Second numerical experiment: reconstruction of two thin objects (e.g., a disconnected crack). Upper row from left to right: initial guess, after 10, and 30 iterations. Central row from left to right: after 40, 50, and 60 iterations. Bottom row from left to right: after 70, 120, and 150 iterations. The reference medium is displayed in the top left image of figure 6.

- [7] Bryan K, Liepa V, and Vogelius M 1993 Reconstruction of multiple cracks from experimental electrostatic boundary measurements, *Inverse Problems and Optimal Design in Industry* **7** 147–167.
- [8] Burger M 2001 A level set method for inverse problems *Inverse Problems* **17** 1327–55.
- [9] Chan T F and Tai X-C 2003 Level set and total variation regularization for elliptic inverse problems with discontinuous coefficients *J. Comput. Phys.* **193** 40–66.
- [10] Cheney M, Isaacson D and Newell J C 1999 Electrical impedance tomography *SIAM Review* **40** 85–101.
- [11] Chung E, Chan T and Tai X.-C. 2005 Electrical impedance tomography using level set representation and total variational regularization, *Journal of Computational Physical* **205** 357–372.
- [12] Dines K A and Lytle R J 1981 Analysis of electrical conductivity imaging, *Geophysics* **46** 1025–1036.
- [13] Dorn O, Miller E and Rappaport C 2000 A shape reconstruction method for electromagnetic tomography using adjoint fields and level sets *Inverse Problems* **16** 1119–56.
- [14] Dorn O and Lesselier D 2006 Level set methods for inverse scattering (Topical Review), *Inverse Problems*, **22**, R67–R131.
- [15] Eggleston M R, Schwabe R J, Isaacson D and Coffin 1989 *The application of electric current computed tomography to defect imaging in metals*, (in Review of Progress in Quantitative NDE, D O Thompson and D E Chimenti, eds., Plenum, New York).
<http://www.athena.uc3m.es/>
- [16] Fang W 2005 Multi-phase permittivity reconstruction in electrical capacitance tomography by level set methods *preprint*.
- [17] Feng H, Karl W C and Castanon D 2000 Tomographic reconstruction using curve evolution *Proc. IEEE Int. Conf. Computer Vision Pattern Recognition, Hilton Head Island, 13-15 June 2000*, Vol. 1, pp 361–66.
- [18] Friedman A and Vogelius M 1989 Determining cracks by boundary measurements *Indiana Univ. Math. J.* **38** 527–556.

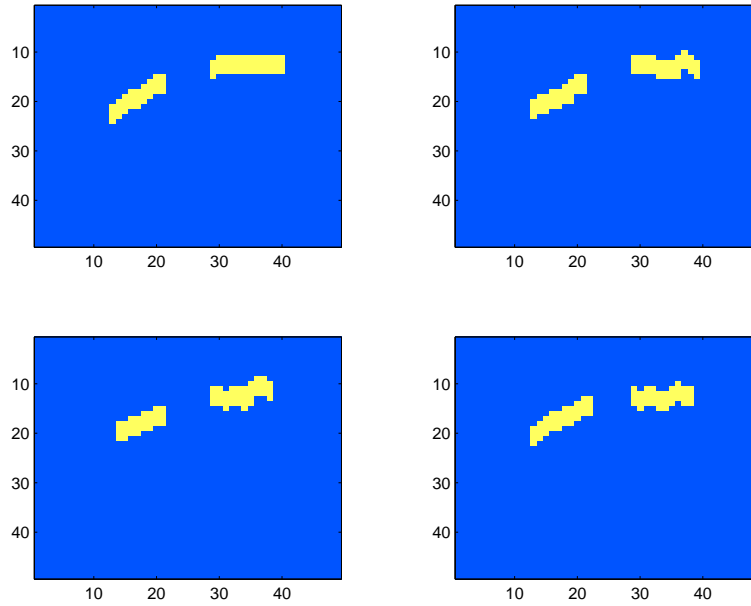


FIGURE 6. Third numerical experiment: final reconstructions (after 200 iterations) of two thin objects for different noise levels σ . Top left: reference medium. Top right: reconstruction without noise. Bottom left: reconstruction with $\sigma = 0.001$. Bottom right: reconstruction with $\sigma = 0.005$.

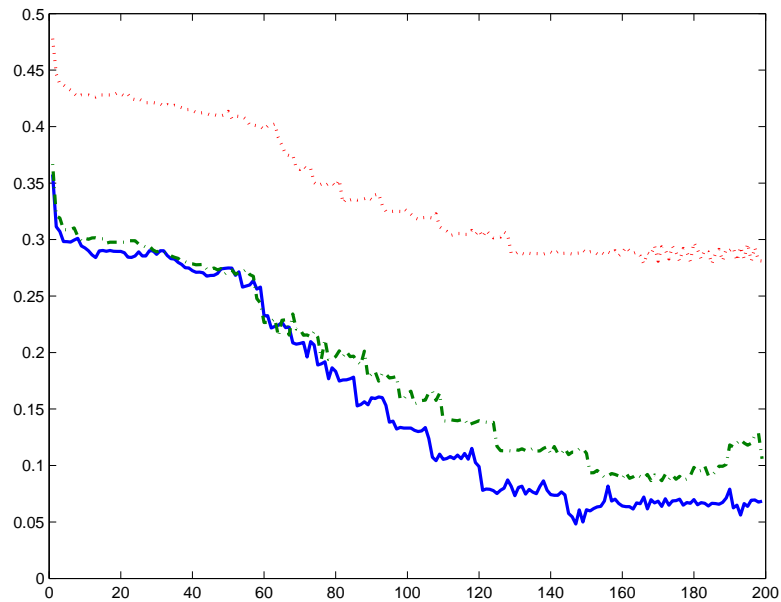


FIGURE 7. Evolution of the least squares cost for different noise levels. Solid line (without noise), dot-dashed line ($\sigma = 0.001$), dotted line ($\sigma = 0.005$).

- [19] Holder, D 1993 *Clinical and physiological application of electrical impedance tomography*, (UCL Press, London).
- [20] Ito K, Kunisch K and Li Z 2001 Level-set approach to an inverse interface problem *Inverse Problems* **17** 1225–1242.
- [21] Kohn R V and Vogelius M S 1985 Determining conductivity by boundary measurements II *Commun. Pure Appl. Math.* **38** 643–667.
- [22] Liepa V, Santosa F and Vogelius M 1993 Crack determination from boundary measurements reconstruction using experimental data, *J. Nondestructive Evaluation* ,**12** 163–174.
- [23] Litman A, Lesselier D and Santosa D 1998 Reconstruction of a two-dimensional binary obstacle by controlled evolution of a level-set *Inverse Problems* **14** 685–706.
- [24] Nachman A I 1988 Reconstruction from boundary measurements *Ann. Math.* **125** 531–576.
- [25] Nachman A I 1995 Global uniqueness for a two-dimensional inverse boundary value problem *Ann. Math.* **142** 71–96.
- [26] Natterer F and Wübbeling F 2001 *Mathematical Methods in Image Reconstruction (Monographs on Mathematical Modeling and Computation Vol. 5)* (Philadelphia: SIAM).
- [27] Osher S and Sethian J A 1988 Fronts propagating with curvature-dependent speed: algorithms based on Hamilton-Jacobi formulations *J. Comput. Phys.* **79** 12–49.
<http://www.athena.uc3m.es/>
- [28] Osher S and Fedkiw R 2003 *Level Set Methods and Dynamic Implicit Surfaces* (New York: Springer).
- [29] Parker R L 1984 The inverse problem of resistivity sounding *Geophysics* **42** 2143–2158.
- [30] Ramananjaona C, Lambert M, Lesselier D and Zolésio J-P 2001 Shape reconstruction of buried obstacles by controlled evolution of a level set: from a min-max formulation to numerical experimentation *Inverse Problems* **17** 1087–1111.
- [31] Rondi L and Santosa F 2001 Enhanced electrical impedance tomography via the Mumford-Shah functional 2001 *ESAIM: Control, Optim. Calculus Variations* **6** 517–38.
- [32] Santosa F and Vogelius M 1991 A computational algorithm to determine cracks from electrostatic boundary measurements *Internat.J.Engr. Sci.* **29** 917–937.
- [33] Santosa F 1996 A level set approach for inverse problems involving obstacles *ESAIM Control, Optim. Calculus Variations* **1** 17–33.
- [34] Sethian J A 1999 *Level Set Methods and Fast Marching Methods* (2nd ed) (Cambridge: Cambridge Univ. Press).
- [35] Soleimani M, Lionheart W R B and Dorn O 2005 Level set reconstruction of conductivity and permittivity from boundary electrical measurements using experimental data *Inverse Problems Sci. Eng.* **14** 193–210.
- [36] Soleimani M, Dorn O and Lionheart W R B 2006 A Narrowband Level Set Method Applied to EIT in Brain for Cryosurgery Monitoring *IEEE Trans. Biom. Eng., in press.*
- [37] Van den Doel K and Ascher U M 2006 On level set regularization for highly ill-posed distributed parameter estimation problems *J. Comp. Phys.* **216**, 707–723.

Grupo de Modelización y Simulación, Universidad Carlos III de Madrid, Spain
E-mail: jdiego@math.uc3m.es